Available online at www.sciencedirect.com
ScienceDirect
Acta Materialia 59 (2011) 451–461
Acta MATERIALIA
www.elsevier.com/locate/actamat

Orowan strengthening at low temperatures in bcc materials studied by dislocation dynamics simulations

G. Monnet [a,*], S. Naamane [a], B. Devincre [b]

[a] EDF – R&D, MMC, Avenue des Renardières, 77818 Moret-sur-Loing, France
[b] LEM, CNRS-ONERA, 29 Avenue de la Division Leclerc, 92322 Chatillon Cedex, France

Received 29 July 2010; received in revised form 16 September 2010; accepted 17 September 2010
Available online 26 October 2010

Abstract

In this paper, the first investigation of the Orowan strengthening mechanism in the thermal plastic regime of body-centered cubic (bcc) materials is made with dislocation dynamics simulations. In bcc crystals, the mobility of dislocations strongly depends on temperature and dislocation line characters. Unlike the classical picture of the Orowan mechanism, simulations show that the difference in mobility between screw and non-screw characters is the key parameter. Simulations at different temperatures and with different precipitate microstructures illustrate the contribution of two mechanisms to Orowan strengthening: a thermally activated mechanism induced by the length dependency of the screw dislocation mobility and an athermal mechanism associated with dislocation line tension. The influence of the particle distribution is studied with a comparison between regular and random particle arrangements. In most cases, distribution effect can be accounted for by calculating effective particle spacing in the screw dislocation directions.

Keywords: Dislocation dynamics; Low temperature deformation; Bainitic steels; Thermally activated processes; Carbides

1. Introduction

When gliding dislocations encounter incoherent or large precipitates in their glide plane, they are usually bypassed according to the Orowan mechanism [1,2]. All the existing investigations of this important mechanism (for a review see Refs. [3,4]) are quasi-static, i.e., they assume that dislocation configurations depend only on the instantaneous value of the shear stress. Hence, dislocation mobility is supposed to be infinite for all dislocation characters. Bacon, Kocks and Scattergood (BKS) developed an important model for Orowan strengthening (OS) [5]. This model predicts the quasi-static OS associated with a random distribution of particles of equal size. It reproduces correctly most of the results of atomistic [6] and dislocation dynamics (DD) simulations [7,8]. However, when the particle distribution is not random or includes particles of different sizes, the BKS model becomes inappropriate. For that reason, Mohles et al. [9,10] made additional investigations of the OS in materials with complex distribution of particle sizes and different types of arrangements. As a general result, a quasi-static approach to OS applies in face-centered cubic crystals, but also in hexagonal close-packed and body-centered cubic (bcc) materials at high temperatures. In the thermal regime of bcc metals, the quasi-static approach falls down, and dynamical effects must be considered. This is because the mobility for screw dislocations (SD) is much lower than for other dislocation characters, as manifested by the strongly anisotropic dislocation microstructures observed in transmission electron microscopy experiments [11,12]. SD motion, hindered by a strong lattice friction, proceeds through nucleation and subsequent propagation of kink pairs. During deformation, long SD are chopped into shorter segments by dislocation–particle interaction. To the knowledge of the authors, only one attempt to model precipitation hardening in this thermal regime has

* Corresponding author.
E-mail address: ghiath.monnet@edf.fr (G. Monnet).

1359-6454/$36.00 © 2010 Acta Materialia Inc. Published by Elsevier Ltd. All rights reserved.
doi:10.1016/j.actamat.2010.09.039

been reported in the literature [13]. The results reported in this paper clearly show that DD in the thermal regime is more complex than previously assumed, and a new model is proposed for OS.

Although the calculations made in this study are specifically dedicated to reactor pressure vessel steels (RPV), a material of interest to the nuclear industry, the results of this study are general and should apply to any materials where the SD mobility is restricted by a strong lattice friction. The simulation methodology used is briefly described in the next section. In particular, the velocity laws used in DD simulation are justified. In the third and forth sections, the OS induced by periodic and random distributions of particles is simulated. The subsequent section is dedicated to discussion and to the presentation of an original model deduced from the simulation results.

2. DD simulations: methodology

Calculations are performed with the DD simulation 'microMegas' (mM) [14]. For a presentation of this code, readers are invited to consult Refs. [15–17]. Here, only the specific rules needed to simulate the Orowan mechanism at low temperature in a bcc crystal are presented. In the simulations, the discretization reference length is taken as a fraction of the curvature radius on the non-SD sections. The latter depends on the temperature and the precipitate density. It was found to vary between 0.4 and 1.0 μm.

Carbide precipitates in RPV steels are represented in the simulation by spherical inclusions in an isotropic continuum with iron elastic properties. Poisson's ratio is assumed constant ($\nu = 0.33$), and the temperature dependence of the shear modulus is listed in Table 1. As a constitutive rule, dislocations are not allowed to penetrate particles, and the stress field induced by carbide inclusions in the iron matrix is neglected. This approximation is adopted for reasons of simplicity and does not alter the main conclusions of this study. When mechanically loaded in single slip conditions, dislocations in system $1/2\langle 1\,1\,\bar{1}\rangle\{0\,1\,1\}$ with Burgers vector $b = 0.248$ nm glide in parallel slip planes. All simulations were carried out at constant imposed plastic strain rate, i.e., the total area swept by dislocations per unit time is kept constant. This leads to an average dislocation velocity of $v = 1\ \mu\text{m s}^{-1}$. A value thought to be the usual velocity of SD in conventional tensile tests [16,18]. As a result of mechanical loading, dislocations surround the particles, hence leading to the Orowan mechanism. The dislocation–particle interactions end up with the formation of Orowan loops hugging the bypassed precipitates.

Distinction is made in the simulation between velocity laws applied to SD and other dislocation characters. Note that the local dislocation line character is deduced from a continuous representation of the dislocation line passing through the center of each discretization segment. Hence, it is independent of the segment direction used to distcretize dislocations in the simulation.

Since SD mobility controls plastic deformation in bcc iron at low temperatures, the flow stress measured in tensile tests on iron single crystal is defined as the stress necessary to move SD at a given average velocity [18,19]. Following an important remark in Ref. [19], attention is paid to distinguishing the initiation of SD glide, from the onset of plastic deformation, which is conventionally defined as the stress recorded at 0.2% strain. From experimental data, a stationary velocity law for SD is defined in Ref. [19] with the form

$$v_s = Hl \exp\left[-\frac{\Delta G_0}{KT}\left(1-\sqrt{\frac{\tau_s}{\tau_0}}\right)\right] \tag{1}$$

where H is constant equal to $1.5 \times 10^{11}\ \text{s}^{-1}$, l the length of the straight SD section, k the Boltzmann constant, T the absolute temperature, and τ_s the effective stress calculated in DD simulations at the center of the SD segment. ΔG_0 and τ_0 are fitting parameters [19] and equal to 0.84 eV and 363 MPa, respectively.

The question of the non-SD mobility (denoted as edge dislocations (ED) in the following for simplicity) is more problematic, as their mobility does not contribute directly to the flow stress [20]. On the one hand, at a given stress, ED are known to glide at a velocity much greater than SD and, on the other hand, ED are known to experience, in materials such as steel, strong interactions with interstitial atoms such as carbon and nitrogen [21,22]. Although, lattice friction on ED decreases rapidly with temperature [23], their interactions with interstitials impose a thermally activated mobility. This is why a phenomenological form is used in the simulation for all non-SD line sections:

$$v_e = v_0 K \exp\left[-\frac{\Delta G_0}{KT}\left(1-\sqrt{\frac{\tau_e}{\tau_0}}\right)\right] \tag{2}$$

where v_0 is a constant equal to $1.5 \times 10^5\ \text{m s}^{-1}$, and K a multiplication factor. Other parameters appearing in Eq. (2) have meanings similar to those in Eq. (1). The numerical evaluation of v_0 and K are based on the following assumptions. First, the velocity of an ED segment is supposed to be K times the velocity of a screw segment 1 μm in length. Secondly, considering experimental evidences, the mobility of all dislocation characters is supposed identical at the beginning of the athermal plateau, and the mobility of ED is much higher than that of SD when the temperature is decreased. The different values for K used in the simulations at different temperatures are listed in Table 1. From previous simulations based on similar types of velocity laws [16,19], it is known that, as long as $K \gg 1$, its value affects neither the dislocation collective properties

Table 1
Temperature dependence of the shear modulus μ and the factor K in the velocity Eq. (2) for non-SD.

	T (K)					
	50	100	150	200	250	300
μ (GPa)	86.71	85.86	85.00	84.16	83.31	82.46
K	10^6	10,000	1000	200	50	1

nor the computed flow stress. Moreover, it must be noted that the simulated dislocation microstructures at low temperature are not very sensitive to K values. Lastly, the OS model developed in this paper is independent of the type of velocity law used for SD.

The particle microstructure used in the simulations is defined with three quantities: the particle diameter (D), their average spacing ($\overline{L}$) and their three-dimensional (3D) spatial distribution. In this study, a constant value of particle size is considered: $D = 100$ nm. This corresponds to the average size of carbides in RPV bainitic steels. Average spacing between particles is explored in the range $0.1 \leqslant L \leqslant 2$ μm, and two different types of particle arrangements are tested: a square periodic and a random distribution.

3. Square periodic distribution of particles

In a square distribution, precipitates are distributed at the nodes of a regular square network in the dislocation glide plane, and the elementary spacing between precipitates is parallel to the mobile dislocations. This configuration is equivalent to modeling the interaction of a straight infinite dislocation line with a periodic row of particles at fixed spacing L. The path for mobile dislocations is then unique, and the inter-spacing between particles equals $L-D$.

At every temperature investigated, $\Delta\tau$, the strengthening induced by the particle distribution, is the difference between τ_{app}, the maximum stress applied during the bypassing process, and the initial stress needed to move a straight segment of reference length l_0 at the same average velocity $v = 1$ μm s^{-1}. This length l_0 is characteristic of the microstructure without particles. It can be, for instance, the average spacing between forest dislocations at a given dislocation density. In other words, l_0 is the average length of the SD segments if there were no precipitates in the crystal. In the present simulations, l_0 is set equal to 4.2 μm, which corresponds to the dimension of the DD simulation box in the screw and ED directions.

Given the mobility laws defined in Section 2, bypassing with SD and ED must be distinguished. Such differentiation is made with the help of the periodic boundary conditions (PBC), using the property that a long dislocation segment crossing the total simulated volume with PBC is geometrically forced to keep on average its initial character. Note that the assembly of square periodic distribution of particles in some specific directions and with particular spacing is also facilitated by PBC.

For the sake of brevity, this section reports only the results obtained for extreme temperature conditions, i.e., 50 and 250 K. Simulation results at intermediate values are found to scale between those two cases.

3.1. The case of ED

Before interacting with particles, a condition of constant strain rate imposes on ED a stress of amplitude τ_e. Then, when the dislocation touches the particles, in order to keep the strain rate constant, the applied stress is increased up to the maximum value corresponding to the critical configurations reproduced in Fig. 1. No substantial differences are observed between the critical shape simulated at 50 K and at 250 K. All in all, at a given particle spacing L, the simulated critical configurations look independent of temperature and similar to the one obtained in the quasi-static simulations [5]. In addition, the simulation strengthening values plotted in Fig. 1c are found to be coherent with the predictions of the BKS model [5], which for a square distribution of particles takes the form:

$$\Delta\tau_{BKS} = A\frac{\mu b}{L-D}\ln\frac{2\overline{D}}{b} \tag{3}$$

In Eq. (3), A is constant equal to $1/(2\pi)$ for ED. $\overline{D} = (DL)/(D+L)$ is the harmonic average of L and D and the factor 2 in the logarithm term accounting for the constant term of $0.7 \approx \ln(2)$, existing in the BKS model [5].

In summary, the thermally activated mobility law defined in the simulation for ED (Eq. (2)) does not lead to results different from that obtained in the athermal simulations and is correctly described with the BKS model. As regards OS, ED dynamics seems to follow the quasi-static behavior found in materials with a low lattice friction.

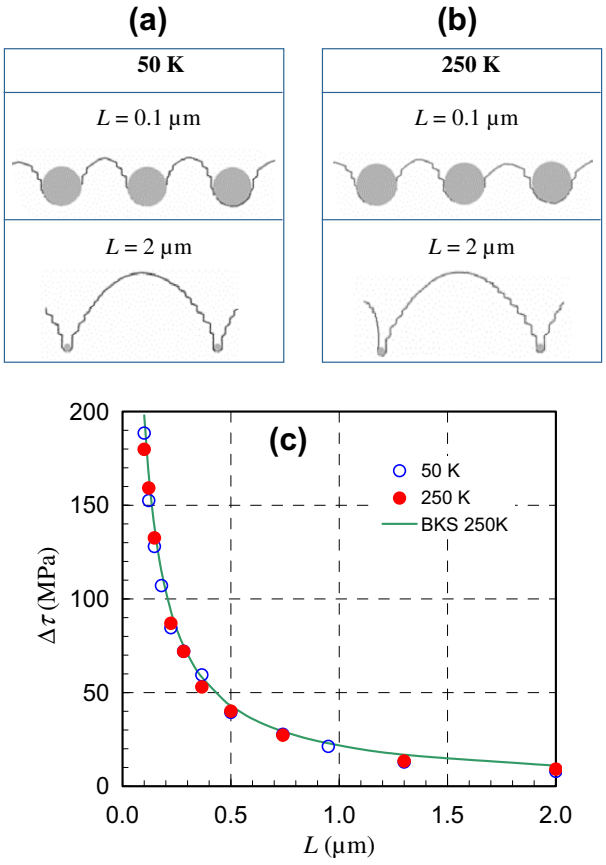

Fig. 1. Critical configuration for ED Orowan bypassing simulated with a square distribution of particles at (a) 50 K and (b) 250 K. OS change as a function of particle spacing (L) and temperature is plotted in (c). The solid line refers to predictions of the BKS model [5].

3.2. The case of SD

The same type of simulations with a SD leads to quite different behavior. As shown in Fig. 2, the critical configurations found at the maximum stress change with the particle spacing and the temperature. Also, the computed OS is found to be systematically lower than the quasi-static prediction made with the BKS model [5].

More precisely, at large values of L and at lower temperatures, Orowan bypassing involves curvature of only small sections of the dislocation line on each side of the particles. At the critical configuration, long straight segments in the screw direction are still observed in between particles. The length l of this screw segment decreases with L or with increasing temperature. At small values of L and higher temperatures, the dislocation lines observed at the critical configuration fully bow-out between the particles.

As illustrated in Fig. 2c, OS is here found to be temperature dependent. At fixed particle spacing L, $\Delta\tau$ always increases with temperature. Furthermore, at large values of L, DD is poorly sensitive to the particle spacing, while at lower spacing L, the OS rapidly evolves.

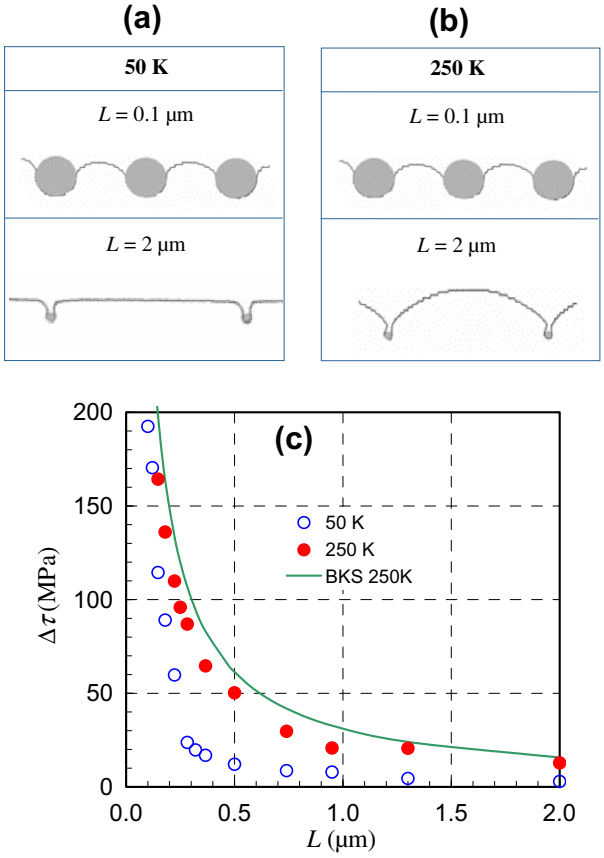

Fig. 2. Critical configuration for SD Orowan bypassing simulated with a square distribution of particles at (a) 50 K and (b) 250 K. OS change as a function of particle spacing (L) and temperature is plotted in (c). The solid line refers to predictions of the BKS model [5].

3.3. Simulation results analysis

The interpretation of the results for ED is relatively simple. The velocity law for an ED segment does not depend on its length. Hence, in the Orowan process, the applied stress must increase only to balance the line tension resistance induced by the dislocation curvature. This line tension effect is independent of the dislocation velocity. The stress τ_e needed to move an isolated straight ED at a given velocity and temperature is therefore a threshold stress. The maximum stress at the critical configuration is then the superposition of the line tension contribution $\Delta\tau_\Gamma$ and the threshold stress τ_e to move a straight ED. OS is reduced consequently to $\Delta\tau_\Gamma$, which is well accounted for in the BKS model (see Fig. 1).

It is interesting to note that one may expect deviation from the BKS model as dislocation segments in the screw direction are formed in the Orowan bypassing process. The low mobility of these segments appearing on each side of the precipitates could delay the formation of Orowan loops and therefore influence OS. In fact, such a feature is not observed in the simulation as an effect of the strong elastic interaction existing between the opposite parts of the dislocation line surrounding a precipitate. Deviation from the BKS model is therefore expected only for large precipitates with a diameter much bigger than that considered in this study.

The analysis for the SD results is completely different. As a SD segment starts to progress between particles, its length decreases, but does not curve. Rather, the dislocation moves forward in a straight manner and forms two curved sections of ED character touching the particles. At the critical configuration, two different behaviors are observed. They are outlined schematically in Fig. 3. When the particle spacing is large and the temperature low, a straight screw segment with finite length l remains at the critical configuration while, for smaller spacing and high

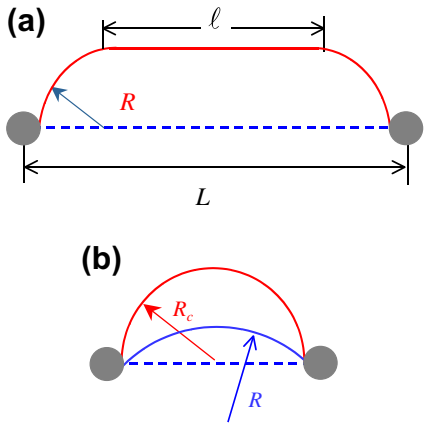

Fig. 3. Schematic drawing of the two types of critical configurations reproduced in the SD simulations: (a) when $L-D$ is larger than twice the radius of curvature R at line sections touching the precipitates; (b) inversely, when the dislocation line is fully curved between precipitates, i.e., when $L-D < 2R$.

temperatures, the dislocation line is fully curved at the critical configuration, and a straight SD section is no longer distinguished. From a geometrical point of view, those two different shapes can be separated by comparing the effective spacing between particles $L-D$ with the radius of curvature R on the non-screw sections, i.e., $L-D>2R$ or $L-D<2R$.

Attention must be paid here to an important observation made during the simulations. When the stress increases up to its critical value, most of the dislocation sections are gliding at the same imposed velocity v. Indeed, the SD segment of length l does not slow down because the stress increases. Furthermore, the curved sections of non-screw character rotate around the particle at a velocity close to that of the screw segment. In the following, it will be considered that all parts of the dislocation move at the same imposed velocity v, except the immobile sections touching the precipitates. As a consequence, it follows from Eqs. (1) and (2) that the effective stresses on SD and ED sections must be different. For the SD, the effective stress equals

$$\tau_s(l)=\tau_0\left(1+\frac{kT}{\Delta G_0}\ln\frac{v}{lH}\right)^2 \tag{4}$$

and for the ED

$$\tau_e=\tau_0\left(1+\frac{kT}{\Delta G_0}\ln\frac{v}{v_0K}\right)^2 \tag{5}$$

Again, it is important to note that in Eq. (5) the effective stress τ_e on ED is a function of K, which has no physical basis. Hence, the relation between τ_e and v is not unique. It is shown in the discussion that this point does not affect the generality of the conclusions.

3.3.1. Critical configurations with $L-D>2R$

As drawn schematically in Fig. 3, for critical configuration with $L-D>2R$, the simulated OS is consistent with a mechanism first described by Louchet et al. [24] and later revised in Ref. [13] in the case of precipitate strengthening. This mechanism directly correlates a deficit of SD segments mobility to a reduction in their length. When interacting with the particles, the SD segment length decreases from l_0 to l. According to Eq. (4), to keep the SD velocity constant, this length decrease leads to an increase in the applied stress, denoted as $\Delta\tau_l$. Such length effect can be calculated from Eq. (4) by differentiating the results for l_0 and l. At the critical configuration, $l=L-D-2R$. In order to evaluate the latter quantity, the radius of curvature R on ED segments must be calculated.

For this purpose, a simple approach is proposed. This reasoning and other important features developed in this section are outlined in Fig. 4. The difference between the effective stress $\tau_s(l)$, which is close to the applied stress τ_{app}, and the effective stress τ_e corresponds to the line tension resistance to the curvature of the ED sections. The latter contribution, $\Delta\tau_\Gamma$, is known to be proportional to $\mu b/R$. The radius of curvature is thus only a function of the difference $\tau_s(l)-\tau_e$. Hence

$$R\approx\frac{\mu b}{\tau_s(l)-\tau_e} \tag{6}$$

The difference between the effective stresses on SD and ED gliding at the same velocity is basically a function of the chemical composition of the material and the temperature. Therefore, R is not constant, and it is material dependent. In the present work, the variation in R as deduced from Eqs. (1) and (2) remains limited.

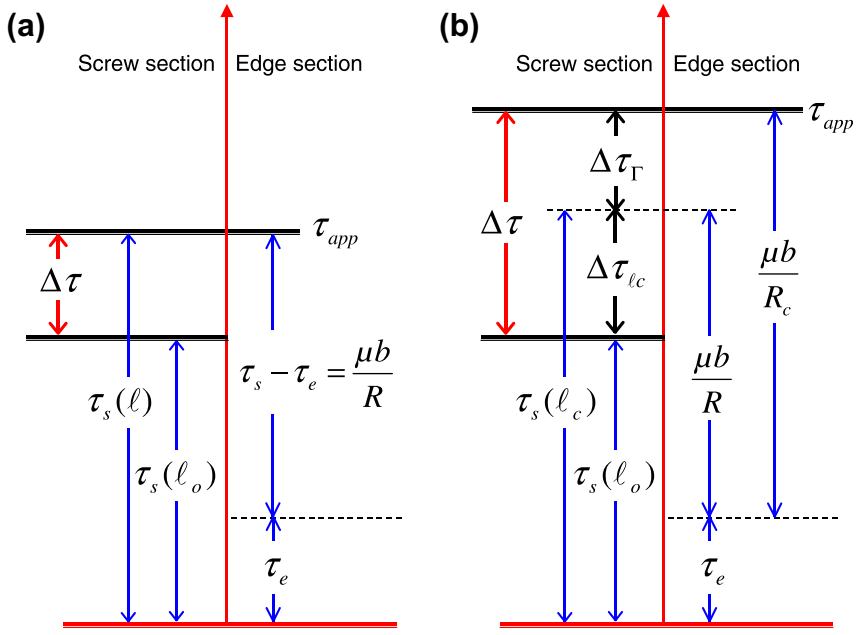

Fig. 4. Schematic drawing of the stress parts contributing to OS in bcc metals at low temperatures. Stress decomposition on SD and on ED is differentiated as well as the case of (a) large and (b) small precipitates spacing.

Using Eqs. (4) and (6), the strengthening $\Delta\tau_l$ associated with the reduction in the SD length from l_0 to l takes the form:

$$\Delta\tau_l = \tau_0 \frac{kT}{\Delta G_0} \ln\frac{l_0}{l}\left(2 + \frac{kT}{\Delta G_0}\ln\left(\frac{v^2}{H^2 l_0 l}\right)\right) \quad (7)$$

Note that, at low temperature, the second term in parentheses becomes small compared with 2, and Eq. (6) takes the simplified form

$$\Delta\tau_l = \tau_0 \frac{2kT}{\Delta G_0} \ln\frac{l_0}{l} \quad (8)$$

This length effect is approximately a logarithmic function of l. Hence, $\Delta\tau_l$ is mainly a logarithmic function of the precipitates density. This quantity is influenced in a complex manner by the difference between SD and ED mobility. One may also notice that this length effect applies in all conditions, since the existence of precipitates always forces a reduction in l. Remarkably, this effect is independent of the shear modulus of the material.

3.3.2. Critical configurations with $L - D < 2R$

The case illustrated in Fig. 3b is now considered, when the SD length l goes to zero on a curved dislocation, i.e., $L - D < 2R$. Following a discussion in Ref. [25], the thermally activated motion of SD is conditioned by the nucleation of kink pairs, which allows SD to jump from one Peierls valley to the next in their glide plane. The determination of the critical size for kink-pair nucleation is a non-trivial problem which requires atomistic calculations. Nevertheless, it is reasonable to assume the existence of a minimum length l_c for SD segments in the order of $10b$ [25,26]. It is checked that the exact value of l_c has a weak influence on DD simulation results, but it mathematically defines a transition between two strengthening mechanisms.

As illustrated in Fig. 4b, the applied stress must first be increased in order to compensate the length reduction in the SD segment from l_0 to l_c. This mechanism is the length strengthening effect discussed in the case of $L - D > 2R$ and denoted as $\Delta\tau_l$. Secondly, from the configuration $l = l_c$ to the critical configuration, the applied stress must be further increased to force the dislocation to glide at constant velocity. This phenomenon originates from the elastic self-interactions taking place on a curved dislocation line. For this reason, it is designated as a line tension strengthening effect and denoted as $\Delta\tau_\Gamma$. The index "s" is added to emphasize the fact that the original character of the dislocation segment is screw.

The evaluation of those two strengthening mechanisms, $\Delta\tau_l$ and $\Delta\tau_\Gamma$, is made as follows. $\Delta\tau_l$ is given by Eq. (8), but replacing l with l_c:

$$\Delta\tau_{lc} = \tau_0 \frac{2kT}{\Delta G_0} \ln\frac{l_0}{l} \quad (9)$$

Eq. (9) is a measure of the maximum stress increment which can be attributed to the length strengthening effect. It is independent of the particle spacing and distribution.

To calculate the line tension effect $\Delta\tau_\Gamma$, the process of Orowan bypassing at $L - D > 2R$ needs deeper investigation. In athermal (quasi-static) conditions, Orowan bypassing is well described by the BKS model (Eq. (3)), and it was demonstrated that this model still applies with ED at temperatures below the athermal critical temperature. However, the case of SD is different (see Fig. 3b), as the resistance associated with line curvature starts to operate only when the length of SD is l_c. This condition is geometrically satisfied when the curved sections on both sides of the particle join each other to form a continuous arc of circle with curvature radius R. At this configuration, the applied stress is $\tau_s(l_0) + \Delta\tau_{lc}$, and the dislocation is not curved enough to bypass the precipitates. The SD must glide further to reach the critical configuration with a radius of curvature R_c. It is essential to note that, during this step, the mobility of the front screw segment no longer depends on its length, since $l = l_c$. So, the curved SD line behaves as in the case of the ED discussed in Section 3.1. Consequently, from this intermediate configuration, the stress increment needed to decrease the radius of curvature from R to R_c must be equal to $\Delta\tau_{BKS}$ (i.e., the quasi-static stress necessary to bow-out a straight SD up to a curvature radius R_c) minus $\Delta\tau_\Gamma(R)$ (i.e., the quasi-static stress necessary to bow-out a straight SD up to a curvature radius R). To summarize, at R_c, the applied stress is at maximum and equals $\tau_s(l_0) + \Delta\tau_{lc} + \Delta\tau_\Gamma$, as sketched in Fig. 4b. From this observation, one deduces:

$$\begin{aligned}\Delta\tau_\Gamma &= \Delta\tau_{BKS} - \Delta\tau_\Gamma(R) \\ &= \frac{\mu b}{2\pi(1-v)}\left(\frac{1}{L-D} - \frac{1}{2R}\right)\ln\frac{2\overline{D}}{b}\end{aligned} \quad (10)$$

In Eq. (10), R is the radius of curvature at $\tau_{app} = \tau_s(l_c)$ and calculated using Eq. (6).

Finally, the total OS, $\Delta\tau_{lc} + \Delta\tau_\Gamma$, for periodic square distribution of precipitates when $L - D < 2R$ is

$$\Delta\tau = \tau_0 \frac{2kT}{\Delta G_0}\ln\frac{l_0}{l_c} + \frac{\mu b}{2\pi(1-v)}\left(\frac{1}{L-D} - \frac{1}{2R}\right)\ln\frac{2\overline{D}}{b} \quad (11)$$

3.3.3. Validation of the model equations

First, the results obtained for the square periodic configuration are summarized. (i) For ED, the OS computed in the simulation is temperature independent and follows the athermal prediction of the BKS model given by Eq. (3). This result comes from the absence of the length effect on the mobility of ED. (ii) For SD, depending on the temperature and the particle spacing, the strengthening is caused only by a length effect (Eq. (8)) or by two mechanisms, a length and a line tension effect (Eq. (11)).

The accuracy of the model equations deduced from the simulation analysis is tested in Fig. 5 by comparison with the DD simulation results. This comparison is made at two different temperatures (50 and 250 K) and the predictions of the BKS model are added for comparison.

In Fig. 5, the frontier between the domains $L - D < 2R$ and $L - D < 2R$ is apparent. The important OS observed

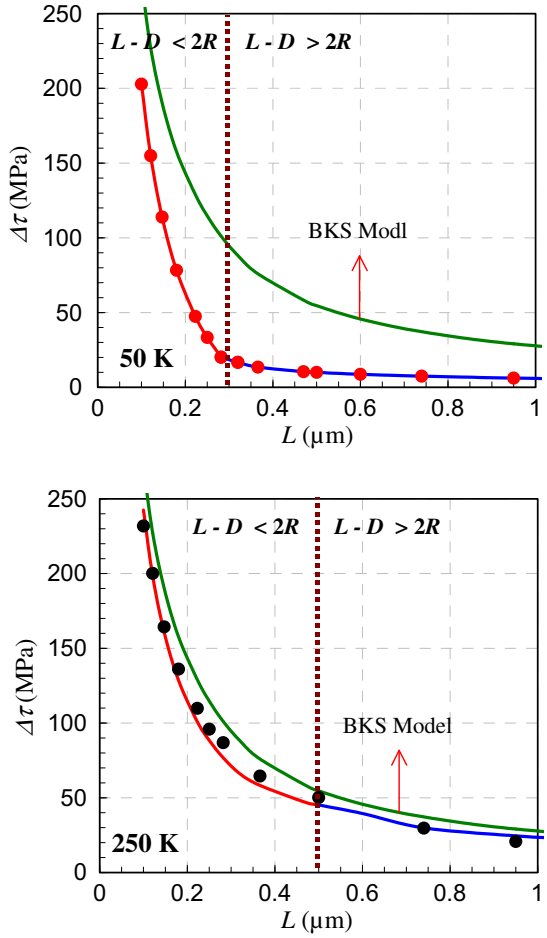

Fig. 5. Comparison at 50 and 250 K between the results of DD simulations with a SD (full circles) and the predictions of Eqs. (8) and (11) (full lines). Vertical dashed line is the limit of both equations validity. Solutions of the BKS model are also reproduced (see arrows) for comparison.

at lower particle spacing is clearly the manifestation of the line tension effect. Inversely, a weak OS is observed when the SD length effect is the only mechanism involved. Globally, the junction of Eqs. (8) and (11) gives a good prediction of the DD simulation results for a periodic square distribution of particles.

4. Random distribution of precipitates

4.1. Simulation conditions

Periodic distributions of precipitates are poor descriptions of real material microstructure. These simulations allows only for a theoretical investigation of the elementary processes involved in particle strengthening mechanisms. Unless the volume fraction of particles is large [4], say more than few per cent, the microstructures observed experimentally always exhibit a random character. Since in the present case the precipitate volume fraction is only 1.6%, the existence of a coalescence phenomenon inducing depletion zones [10] can be neglected. DD simulations accounting for 3D random distribution of particles require considering a large volume element, hence a large number of dislocations and particles. This is why such calculations are sometime referred as "mass simulations". Given the time necessary to undertake DD mass simulations, this study is restricted to the description of a realistic microstructure of carbides in RPV steels. Consistently with the calculations made in the previous section and with experimental observations [8], the diameter of carbides is set to $D = 100$ nm and their density $\rho \approx 3 \times 10^{19}$ m^{-3}. This density corresponds to a surface density $\rho_s = D\rho = 3 \times 10^{11}$ m^{-2} and to an average planner spacing $\lambda = 1/\sqrt{\rho_s} = 0.57$ μm.

All the simulations reported in this section were carried out in single slip condition and at a constant strain rate. The simulated volume has dimensions $5 \times 3 \times 3$ μm^3, and PBC are applied. Attention has been paid to start the simulations with a realistic dislocation microstructure at each temperature. Indeed, when simulations in the thermal regime are started with isotropic dislocation microstructures, ED sections move first, and they accommodate a large amount of plastic deformation before the onset of the SD motion [27,28]. Taking into account the limited amount of plastic deformation that can be reproduced in mass simulations, this solution is obviously unfavorable. This is why, at every investigated temperature, a pre-deformation is applied to the simulated volumes free of particles. During this first calculation, a random microstructure of small dipolar loops is loaded to multiply the dislocation density significantly. As an effect of the difference in SD and ED mobility (Eqs. (1) and (2)), a strongly anisotropic microstructure is then generated. This preliminary calculation is stopped when the dislocation density on the primary slip system reaches the reference value 10^{12} m^{-2}. The value of the imposed strain rate is fixed so that the average velocity of SD is 1 μm s^{-1}, i.e., the same velocity imposed in Section 3. Note that the dislocation microstructure obtained at this point is made mainly of long straight SD.

Then, two independent DD simulations are run at each temperature. This is because the dynamics of dislocations in a matrix with or without particles must be calculated. The difference in flow stress between those two simulations is by definition the OS.

4.2. Simulation results analysis

As in the previous simulations with the square periodic distribution for SD, dislocation–particle interactions are found to change in the random distributions with temperature. Such evolution is illustrated through the picture of the dislocation microstructures simulated at 50 and 250 K. From Fig. 6, it is clear that dislocations are curved at 250 K, while most of the dislocation density is made of long straight SD segments at lower temperatures. In both cases, the DD is a continuous and smooth process. All dislocations are pinned and glide almost at the same velocity.

The stress–strain curves calculated with a random particle distribution are reproduced in Fig. 7a. At every temper-

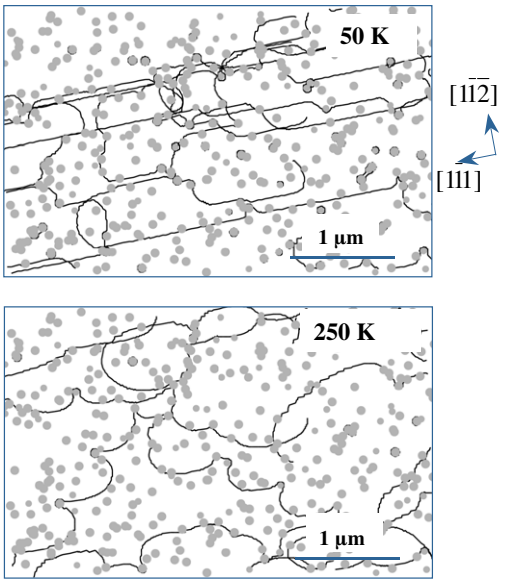

Fig. 6. Examples of loaded simulated dislocation microstructures at 50 and 250 K in thin foils extracted from the simulated volume in a direction parallel to the primary slip system. The particles density is 3×10^{19} m^{-3}, and their diameter is $D = 100$ nm. The more the temperature is decreased, the more the dislocation segments are oriented in the screw direction.

ature, the stress–strain curves start with a rapid increase in the applied stress followed by a plateau. The applied stress at the plateau smoothly fluctuates around a well-defined average value. The latter value is defined as the material flow stress. At each temperature, OS can then be calculated as the difference between the simulated flow stress with and without particles. Results of those calculations are plotted in Fig. 7b.

From Fig. 7b, it is clear that a significant reduction in the OS is observed with decreasing temperature. At 250 K, OS is already decreased by 45% with respect to the result obtained for the same microstructure in athermal condition [8,29]. This effect is remarkable, since all dislocation sections look curved at this temperature. The decrease in OS with temperature is a general result and is independent of the mobility law used for the ED used in the simulation. This is because basically only the SD density controls OS at low temperature. This result is consistent with the well-known observation that in single-phased bcc crystals, the flow stress is controlled only by the SD mobility [27,28].

As the dislocation microstructure at low enough temperatures is made mostly of long SD segments, an option to reproduce mass simulation with a simplified dislocation microstructure can be explored. Simulations with the same microstructure were repeated, but considering only SD. Again, use is made of the possibility offered by PBC in the DD simulation to construct infinite SD. For those calculations, the imposed strain rate was changed to account for differences in the mobile dislocation density and in order to keep the constant dislocation velocity of 1 μm s^{-1}. Results of this second round of computations are reported

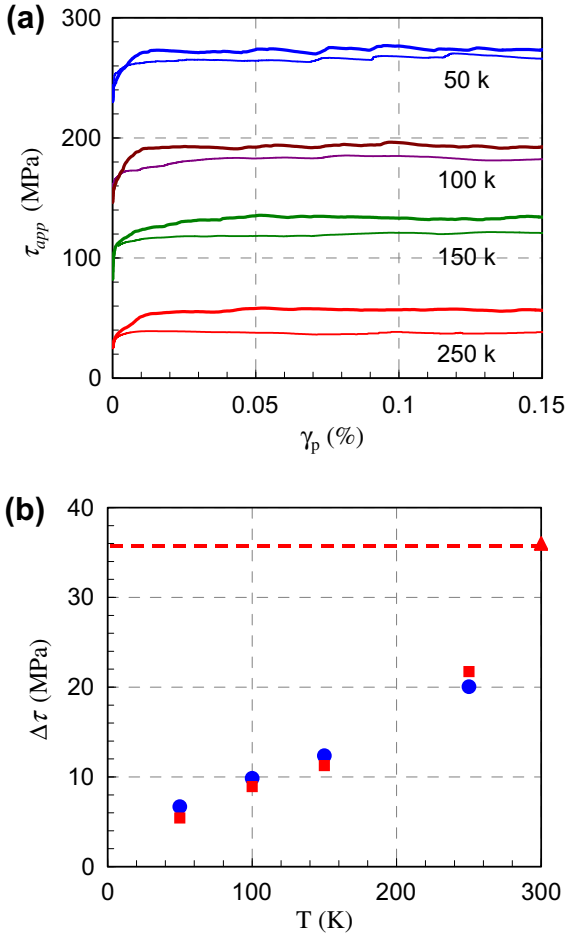

Fig. 7. (a) Simulated stress–strain curves in iron as a function of temperature with (bold lines) and without (thin lines) a random distribution of particles. (b) The OS, $\Delta\tau$, calculated with the square periodic (full squares) and a 3D random (full circles) distribution of particles. The dashed line indicates the athermal strengthening expected from the BKS model and well reproduced with the simulation at the athermal plateau (full triangle).

in Fig. 7b. As good agreement is found with the previous mass simulations, it is demonstrated that SD control the OS. This is why, the SD model developed for periodic particle distributions can be adapted to mass simulation.

4.3. Modeling of mass simulations

Here, an infinite SD interacting with particles randomly distributed in the dislocation glide plane is considered. During its progression, this dislocation line is periodically pinned at particles, and ED sections with a radius of curvature R are formed on each side of the particles.

As illustrated in Fig. 8a, a SD segment of average length $\bar{l}$ pinned between two particles will statistically attain another particle once the dislocation sweeps an area A. In the stationary regime, this area A is related to the average spacing between particles in the dislocation glide plane [24], and equals $A = \lambda^2 = \bar{L}(R + D/2)$. This statistical approach is general and was initially defined in the context

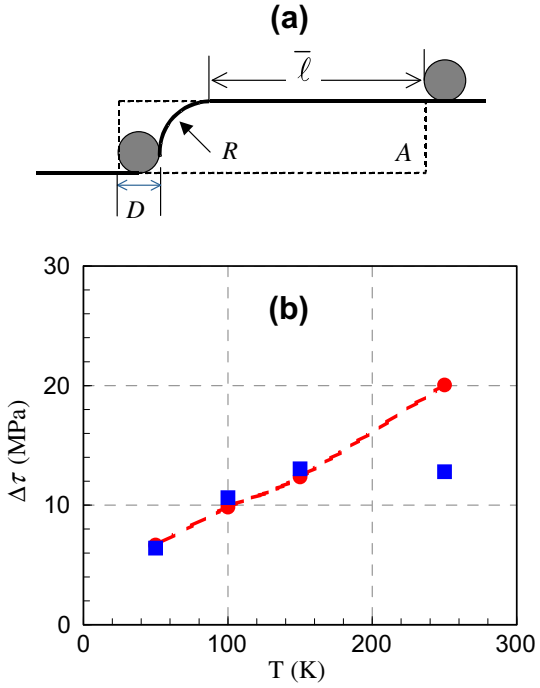

Fig. 8. (a) Schematic drawing of the definition of the average area A in dislocation glide planes associated with each particle in the random distribution. (b) Comparison between the OS calculated with DD simulations (filled circles interpolated by a dashed line) and the solutions predicted with the new model developed in this paper (filled squares).

of the forest hardening for bcc metals [24,30,31] and for precipitate strengthening [13]. In this context, $\overline{L}$ is the average spacing between particles in the screw direction, and this quantity enters the calculation of $\overline{l} = \overline{L} - D - \overline{R}$. This quantity is essential and allows the definition of a modified Eq. (8) to evaluate the SD length effect in a random particle distribution.

The radius of curvature R on the ED segments is not a function of the particle arrangement and therefore Eq. (6) still applies for a random particle distribution. Given the nature of the mobility laws used in the simulations, R does not change notably with temperature. Then, for the sake of simplicity, a constant average value for $\overline{R} \approx 150$ nm is defined which gives $\overline{L} = 1.5$ μm, in good agreement with the observations made in the simulations. This statistical evaluation suggests two important remarks. First, $\overline{L}$ is substantially larger than the average planar spacing between particles $\lambda = 0.57$ μm. Hence, at a fixed particle density, one expects OS with a random distribution to be weaker than in periodic distributions. Secondly, confirmation is made that the simulated random distribution of particles verifies the condition $\overline{L} - D > 2\overline{R}$. This result legitimates the use of Eq. (8) to model OS as a function of temperature.

The results of Eq. (7), replacing l by $\overline{l}$, are plotted in Fig. 8b for comparison with the mass simulation results. The predictions of this equation are in good agreement with the simulations at most temperatures. An overestimation of few MPa is only found at 250 K. A simple model for OS in the thermal regime is then proposed for particle distributions that mimic those observed in RPV steel. This model is free of any adjustable parameter. The small discrepancies observed at 250 K are probably an effect of the curvature on SD found in the simulation at this temperature. Indeed, as illustrated in Fig. 6, at 250 K the difference between the SD and the ED mobility is reduced enough to simulate curved dislocation between precipitates and therefore the use of Eq. (7) is no longer justified.

5. Discussion

The DD simulations and the corresponding model equations developed reveal important physical features for the OS. In materials with a high lattice friction, as in bcc crystal at low temperature, the OS is weak and increases with temperature. In the thermal regime, OS is controlled mainly by the SD mobility, but precise calculations of this strengthening must account for the existing curvature on dislocation sections touching the precipitates. This curvature is proportional to $\tau_s(l) - \tau_e$, where $\tau_s(l)$ and τ_e are the effective stresses needed to move SD and ED at the same velocity, respectively. From Eqs. (4) and (5), it is clear that this effective stress is a function of the imposed dislocation velocity v, the temperature and the mean length $\overline{l}$ of straight SD segments. In general, $\tau_s(l)$ is close to the applied stress, while τ_e depends strongly on the material chemical composition. For instance, in pure metals where the lattice friction on ED is small, the curvature is high and the radius of curvature is well approximated by $\mu b/\tau_{app}$. In other materials such as RPV steel, i.e., in solid solutions with a large concentration of impurities, τ_e is not necessarily negligible compared with $\tau_s(l)$. Louchet and Kubin reported an experimental evidence of this effect [32]. They observed by electronic microscopy in Mo–Nb alloys that the curvature of non-SD is not only a function of the applied stress. Instead, they provided a phenomenological formula similar to Eq. (6) to account for the friction stress on ED.

In addition, at smaller particle spacing, a line tension contribution to OS is observed. A conjunction of a SD length effect and a line tension effect was previously discussed for bcc materials in the context of forest hardening [31]. The line tension effect discussed in the present paper is fundamentally different from that initially proposed by Rauch [30] and used in Ref. [31]. Here, the curvature on non-SD sections does not significantly restrict the mobility of straight screw segments. Line tension appears only at very small spacing when initially SD becomes completely curved.

Also, the detail relation between length effect and a line tension effect is clarified. In contrast to the simple assumption made in Ref. [31] that the two mechanisms always coexist with distinct intensity, the present simulations show that a transition exists between two regimes. The length effect is the dominant mechanism, as it always exists, and it is the one initially restricting the mobility of the dislocations touching precipitates. Then, for the microstructures where $L - D < 2R$, the length effect is found to saturate,

and the line tension effect starts to operate. A line tension effect is then expected only in small particle spacing conditions or when the applied stress is low, i.e., at temperatures approaching the athermal critical temperature.

The decrease in OS with decreasing temperature as reproduced in the simulations is thought to be a general tendency and should apply as long as the SD mobility is much lower than the mobility of ED. Indeed, modifications of the simulation parameter $K(T)$ poorly affect the simulation results.

The model developed in this paper allows an extrapolation of the simulation results to asymptotic behaviors. An important case is, for instance, when $\tau_s(l) \gg \tau_e$, i.e., in the case of pure metals. Then the solution obtained with a random distribution of particles simplifies as follows. First, the radius of curvature (Eq. (6)) becomes only a function of the effective stress on SD, which is close to the applied stress, $\tau_s(l) \approx \tau_{app}$. The radius of curvature becomes equal to $R = \mu b/\tau_{app}$. In such conditions and considering particle distributions where the line tension effect is not expected ($\overline{L} - D \gg 2\overline{R}$), the effective spacing between particles becomes

$$\overline{l} = \frac{1}{D\rho\left(\frac{\mu b}{\tau_{app}} + \frac{D}{2}\right)} \tag{12}$$

Inserting Eq. (12) in Eq. (8), one can finally express the OS in bcc pure metals as

$$\Delta\tau = \tau_0 \frac{2KT}{\Delta G_0} \ln\left(\rho D l_0 \left(\frac{\mu b}{\tau_{app}} + \frac{D}{2}\right)\right) \tag{13}$$

Eq. (13) shows that, at a given temperature, the OS depends logarithmically on the density of particles and on the particle size. Such behavior is different form the predictions of most existing theoretical models [4]. Also, when the temperature is decreased, the OS decreases because of the decrease in the pre-logarithmic term of Eq. (13), but also as a result of the fast increase in the flow stress in the logarithmic term.

Lastly, it must be noted that only planar slip is considered in the simulation, and the effect of wavy slip on precipitates bypassing is not taken into account. The influence of wavy slip was observed experimentally and is discussed in Ref. [13]. In the Orowan bypassing process, as a consequence of the accumulation of kinks with opposite sign on both sides of obstacles, the formation of Orowan loops is not observed but, rather, particules articles are bypassed with the formation of a "hairpin" dipole configurations. The existence of this mechanism does not modify the conclusions of this work. This is because, the reported calculation of the OS is based on a critical configurations analysis independent of the details of the bypassing process.

6. Conclusions

The definition of two mobility laws for SD and ED in DD simulations allows for the study of OS in bcc materials at low temperature. Whatever the mobility law used for ED, which is poorly known in many materials, important conclusions can be drawn from the DD simulations and from the corresponding model:

(1) The athermal or quasi-static OS is always larger than the OS found at low temperature.
(2) In the thermal regime, the OS decreases with decreasing temperature and is expected to vanish at OK.
(3) The more the mobility of SD and ED are different, the more OS is reduced.
(4) The OS in the thermal regime is controlled by two elementary contributions: a length effect and a line tension effect.
(5) The length effect results form the decrease in the effective length of SD when interacting with particles. It is always present and is independent of the shear modulus.
(6) The line tension effect contributes to the OS only in the case of small particle spacing and at low flow stresses. In those conditions, it is an additional strengthening contribution to the length effect, which starts when the latter is saturated.
(7) When the mobility of ED is very high, as in pure metals, the OS can be predicted with a simple form (Eq. (13)). From this equation, prediction is made that the OS in the thermal regime varies logarithmically with the particle size and density and decreases strongly with decreasing temperature.

References

[1] Orowan E. Symposium on internal stresses in metals and alloys. Institute of Metals, London; 1948. p. 451.
[2] Mott NF, Nabarro FRN. Proc Phys Soc 1940;52:86.
[3] Friedel J. Dislocations. Oxford: Pergamon; 1964. p. 31.
[4] Nembach E. In: Particle strengthening of metals and alloys. New York: J. Wiley; 1997.
[5] Bacon DJ, Kocks UF, Scattergood RO. Philos Mag 1973;28:1241.
[6] Bacon DJ, Osetsky YN, Rodney D. In: Dislocations in solids, vol. 15; 2009. p. 1.
[7] Monnet G. Philos. Mag. 2006;86:5927.
[8] Queyreau S, Monnet G, Devincre B. Acta Mater 2010;58:5586.
[9] Mohles V, Nembach E. Acta Mater 2001;49:2405.
[10] Mohles V, Fruhstorfer B. Acta Mater 2002;50:2503.
[11] Christian J. Metall Trans A 1982;14:1237.
[12] Louchet F, Kubin LP. Acta Metall 1975;23:17.
[13] Charleux M, Livet F, Bley F, Louchet F, Brechet Y. Philos Mag. A 1996;73:883.
[14] See "mM" home page at: <http://zig.onera.fr/mm_home_page>.
[15] Devincre B, Kubin L, Lemarchand C, Madec R. Mater Sci Eng A 2001;309:211.
[16] Monnet G, Devincre B, Kubin LP. Acta Mater 2004;52:4317.
[17] Queyreau S, Devincre B. Philos Mag Lett 2009;89:419.
[18] Tang M, Kubin LP, Canova GR. Acta Mater 1998;46:3221.
[19] Naamane S, Monnet G, Devincre B. Int J Plasticity 2010;26:8.
[20] Kubin LP. Rev Deform Behav Mater 1976;1:243.
[21] Tapasa K, Osetsky YuN, Bacon DJ. Acta Mater 2007;55:93.
[22] Clouet E, Garruchet S, Nguyen H, Perez M, Becquart C. Acta Mater 2008;56:3450.

[23] Osetsky YuN, Bacon DJ. Model Simul Mater Sci Eng 2003;11:427.
[24] Louchet F, Kubin L, Vesely D. Philos Mag A 1979;39:433.
[25] Hirth JP, Lothe J. Theory of dislocations. New York: McGraw-Hill; 1982.
[26] Domain C, Monnet G. Phys Rev Lett 2005;95:215506.
[27] Solomon HD, McMahon CJ. Metallurgical society conference, vol. 46. New York: Gordon & Breach; 1966. p. 311.
[28] Brown N, Ekvall RA. Acta Metall 1962;10:1101.
[29] Queyreau S, Monnet G, Devincre B. Int J Plasticity 2009;25:361.
[30] Rauch EF. Key Eng Mater 1994;97–98:371.
[31] Tang M, Devincre B, Kubin L. Model Simul Mater Sci Eng 1999;7:893.
[32] Louchet F, Kubin L. In: Proc fifth int conf on high voltage electron microscopy; 1977. p. 423.